frontiers | Frontiers in Materials

TYPE Original Research
PUBLISHED 05 November 2024
DOI 10.3389/fmats.2024.1387699

OPEN ACCESS

EDITED BY
Senthilkumar Krishnasamy,
PSG Institute of Technology and Applied Research, India

REVIEWED BY
Xiaoming Chen,
Xi'an Jiaotong University, China
Kaushik Parida,
Indian Institute of Technology Roorkee, India

*CORRESPONDENCE
Zheyu Hu,
huzheyu1218@163.com

RECEIVED 18 February 2024
ACCEPTED 23 October 2024
PUBLISHED 05 November 2024

CITATION
Hu Z, Zhang D and Zhou Y (2024) 2D heterostructures of graphene oxide and MoS_2 to improve sensitivity performance of flexible pressure sensor with shell biological structure. *Front. Mater.* 11:1387699.
doi: 10.3389/fmats.2024.1387699

2D heterostructures of graphene oxide and MoS_2 to improve sensitivity performance of flexible pressure sensor with shell biological structure

Zheyu Hu*, Dabing Zhang and Yuning Zhou

School of Mechanical Engineering and Mechanics, Xiangtan University, Xiangtan, China

Inspired by the multilayer structure of the shellfish, a novel two-dimensional (2D) composite structure consisting of graphene oxide, MoS_2 and graphene oxide (G/M/G) was integrated to the flexible pressure sensing. The composite structure was prepared by the vacuum suction filtration in order to imitate the high toughness of shellfish. Based on the strategy of strain engineering, a comprehensive experimental bench capable of meeting different strain conditions was connected to a push–pull meter and an LCR digital bridge, and then a computer was used to record the changes in transducer capacitance when an external load was applied to the meter. Graphene oxide (GO) and G/M/G supercells were constructed, and density functional theory (DFT) simulations of the initial energy band structure under strain-free conditions were carried out to determine the relationship between the band gap, conductivity, capacitance, and sensitivity of the G/M/G structure based on band gap theory, and to easily understand the mechanism of the shellfish heterostructure leading to enhanced sensitivity of the sensors. Using two-point bending and axial tensile tests, a flexible pressure sensing device was designed to realize positive strains in the ranges of 0%–5 % and 5%–50 %. The results show that the sensitivity of both GO and G/M/G capacitive pressure sensors decreased with increased strain, and the sensitivity of the G/M/G sensors was significantly improved by 75%–102 % compared to the GO sensors at the same strain. The parallel-plate capacitor model and crack growth theory well explain the experimental results at small and large strains. Our results provide new concepts for the design of novel flexible sonar with high sensitivity and large strain operating range by a simple vacuum filtration method, which can be extended to the design of other high-performance 2D flexible electronic devices.

KEYWORDS

2D heterostructure, shellfish structure, pressure capacitive sensor, strain engineering, density function theory

1 Introduction

Nature has evolved over the 3.8 billion years, since life is estimated to have appeared on the Earth. Evolution has produced objects with the high performance of biomaterials and surfaces formed from the complex interactions between surface

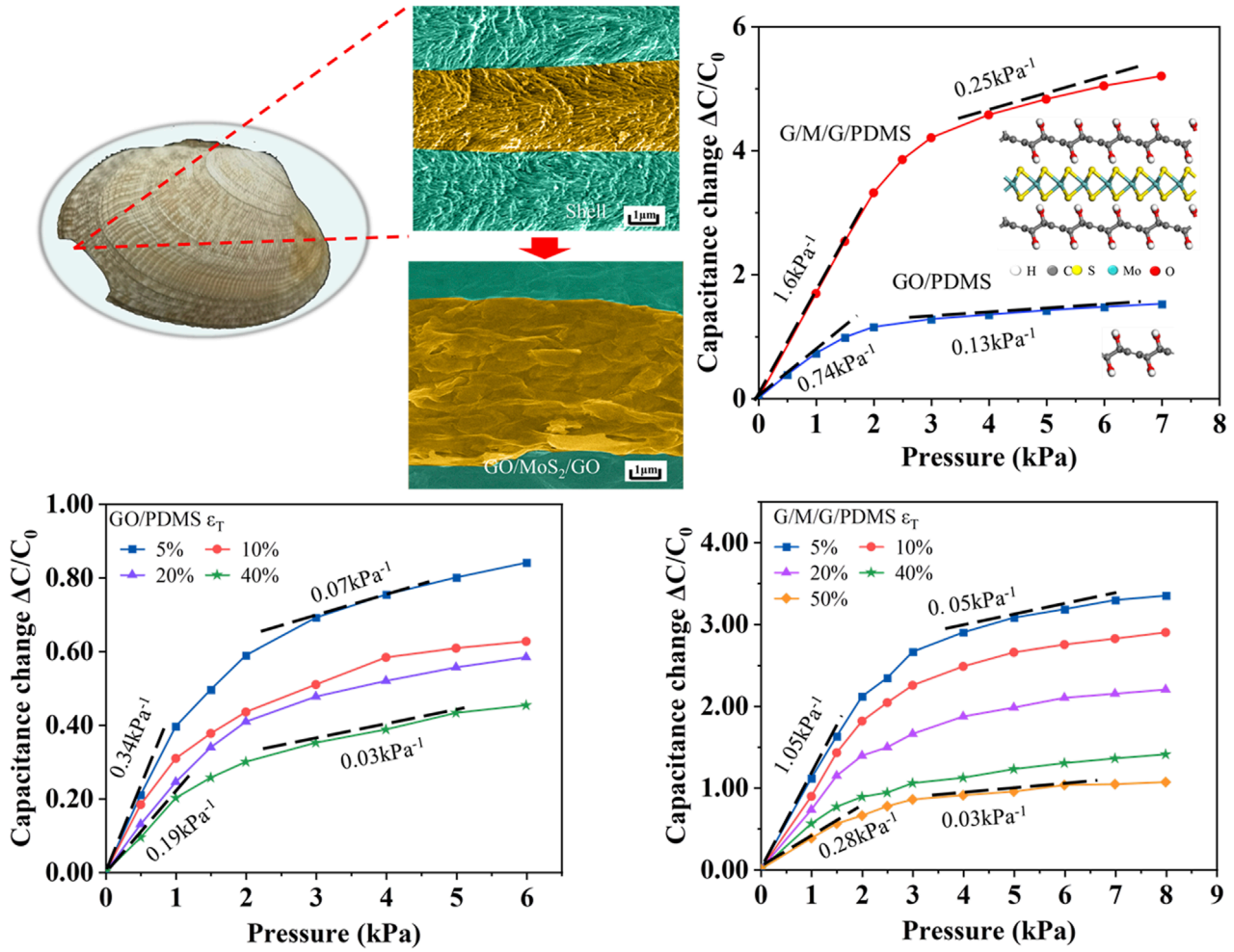

GRAPHICAL ABSTRACT
Inspired by the multilayer structures of shellfish in nature, we constructed a GO/MoS_2/GO heterojunction pressure sensor. The working range under strain and the pressure sensitivity of this new bio-inspired sensor were respectively improved by 25% and 102% compared to the traditional GO sensor structure.

morphology and physicochemical properties, and the emerging field of biomimicry allows the development of nanomaterials and nanodevices by mimicking biology or nature (Bhushan, 2009). Learning from nature has inspired scientists to design novel materials with unique functionalities, such as artificial stimulus-response systems inspired by the ability of chameleons and zebrafish to change their appearance (Isapour and Lattuada, 2018), based on beetle-inspired gradient slant structures (GSS) to endow capacitive pressure sensors with extensive linearity range and excellent sensor-to-sensor uniformity (Wu et al., 2024), stable and economical catalysts inspired by the active sites of enzymes in bioenergy processes (Artero, 2017), and optoelectronic devices with ultra-high optical conductivity inspired by colorful seashells (Sun et al., 2019). Experiments have proved that bio-inspiration is very effective for material innovation, through rational material selection and structural design to achieve better performance by imitating the structure and function of biological entities (Zhang et al., 2016; Wegst et al., 2015).

Recently, shells with a solid surface, such as conch, pearl oyster, and snail, have attracted increasing interest due to their unique structure and remarkable properties (Mao et al., 2016). For example, the pearly structure of shellfish shells, which consists of thin aragonite slabs alternating with biopolymers, has inspired the design of tough materials from fragile, raw materials, such as in the case of mother-of-pearl composites, which are much stronger and tougher than single materials (Jiang and Park, 2014). At the microscale, the ripples of the tablet will gradually lock, harden, and undergo nonlinear deformation dif usion around cracks and defects, providing the pearl layer with extremely high toughness. Unfortunately, the preparation of pearl-like nanomaterials usually requires high-temperature or high-pressure mineralization processes, which causes difficulties in the design and production of such materials. Although molecular dynamics modeling and experimental measurements have confirmed the excellent mechanical properties of shell-like structures, they are still far from being available for use in practical applications.

Recent developments in electronics have focused on flexible devices, which have been widely applied in various fields, including wireless health monitoring, electronic skin, flexible

sensor networks, artificial muscles, flexible human–computer interfaces, and engineered tissue constructs (Huang et al., 2014). A number of flexible pressure sensors have been reported recently, including microstructured layered rubber dielectric capacitors (Mannsfeld et al., 2013), organic field-effect transistors (Takei et al., 2010; Schwartz et al., 2013), organic microstructure piezoresistors (Pan et al., 2014), carbon nanotube-based resistive strain sensors (Michelis et al., 2015), reduced–graphene oxide flakes (Park et al., 2016; Chun et al., 2015), and nanowire arrays (Ha et al., 2015), which can divided into three categories, capacitance, piezoresistivity, and piezoelectricity. Embedded resistive elements demonstrate excellent monitoring performance and failure warning capabilities, but the inclusion of foreign sensing elements may degrade the mechanical properties of the composite and potentially increase the risk of damage and failure (Chen et al., 2023a). Traditional inorganic piezoelectric ceramics are of poor toughness, high stiffness and low durability, and therefore have limited applications in conformal wearable electronics. In this context, piezoelectric nanocomposites are introduced in the piezoelectric sensors to meet the requirements of lightweight, flexibility, processability and biocompatibility. However, agglomeration of high concentration of nanofillers and high viscosity of the resulting mixtures lead to sacrificed mechanical strengths and poor capability of stress transfer from low stiffness polymer matrix to piezoelectric nanofillers. This in turn, produces much lower piezoelectric response than pure inorganic piezoelectric materials. Furthermore, high stiffness nanocomposites caused by high loadings of inorganic nanofillers suppress their processability and restrict their applications in lightweight, portable, and conformal sensors (Zhang et al., 2020). Compared with piezoresistive and piezoelectric sensors, capacitive pressure sensors have the advantages in terms of simple structure, excellent stability, high sensitivity, and low power consumption (Lee et al., 2015). In addition, it is more valuable to develop capacitive sensors than resistive sensors considering that they are more compatible with wireless detection systems, and thus the detection based on change in capacitance has been widely applied in the field of pressure sensing (Yang et al., 2019; Qin et al., 2021). Existing flexible capacitive sensors and devices have difficulties in achieving large strain range and high sensitivity simutaneously (Nesser and Lubineau, 2021; Gao et al., 2022). The effective relative dielectric constant of the sensor is critical to the sensitivity, as it varies with the applied stress. Therefore, it is a viable way to develop new dielectric materials with suitable structures to improve the sensitivity (Li et al., 2020).

Various functional materials have been used in strain and motion sensors, such as [P(VDF-TrFE)] sponge (Parida et al., 2017), carbon nanofibers (Pang et al., 2012) and MXene-coated glass fiber (Chen et al., 2023b). As a new type of carbon material with a flexible 2D structure, graphene has excellent stability in lattice structure and mechanical flexibility, which facilitates the application of graphene-based materials in various flexible sensors (Zhu et al., 2017). Graphene oxide (GO) foam, as a novel building block for future wearable electronic devices, exhibits both excellent elastic properties and high relative dielectric permittivity. It is reported that GO-based sensors can detect a subtle pressure of ~0.24 Pa with a fast response time of 100 m and high sensitivity of 0.8 kPa^{-1} (Wan et al., 2017). However, the detection range and sensitivity of GO pressure sensors in strain environment greatly restrict their applications in flexible sensing (Xu et al., 2018; Cao et al., 2021), and how to integrate the advantages of high sensitivity, wide detection range, excellent durability, and lower limit of detection is still a challenge in developing wearable sensors (Troullier and Martins, 1991; Kresse and Hafner, 1993).

Inspired by nature, two-dimensional heterostructures with shellfish-like structures were prepared by GO and MoS_2 dispersions with the expectation of improving the sensitivity of flexible pressure sensors based on the excellent mechanical properties of the bionic structures. Unlike the traditional high-temperature or high-pressure calcination methods, the vacuum suction filtration method can easily obtain different material combination structures at room temperature, so 2D GO and MoS_2 dispersions can be poured into vacuum suction filters sequentially to obtain 2D materials with GO/MoS_2/GO (G/M/G) heterogeneous structures. Based on the strategy of strain engineering, sensing devices on flexible PDMS plate were constructed by dielectric layering of G/M/G and GO filter films and silver electrodes that were connected with an LCR digital bridge and a push–pull gauge to measure changes in capacitance under different external loads. The superiority of the bionic structures was verified by comparing the pressure capacitance response sensitivity of G/M/G and GO sensors, and the sensitivity variation mechanisms under different strain were studied based on band theory, parallel plate capacitor model, and crack growth theory.

2 Materials and methods

2.1 2D materials

Inspired by the shellfish structure (Figure 1A), 2 mg/mL of an aqueous colloidal suspension of single-layer GO without surfactants and 0.1 mg/mL of single-layer molybdenum disulfide dispersion (Suzhou Tanfeng Graphene Technology Co., Ltd., and Xfnano Materials Tech Co., Ltd.) were used in this study to prepare a 2D heterostructure. They were filtered to form a film after being dried in a vacuum oven for 5 min (Figures 1B, C). The diluted GO dispersion solution was poured into a vacuum filter (Tetrafluoro, Mingjie Instruments, China), and vacuum suction filtration was performed by using a water system filter membrane with a pore size of 0.22 μm at a rate of 60 L/min. After the GO was tightly covered on the filter membrane, the MoS_2 dispersion was slowly poured into the vacuum filtration device, and the suction filtration process was repeated. Finally, the diluted GO dispersion was poured into the vacuum filtration device again, and a layered two-dimensional heterogeneous structure was obtained.

2.2 Characterization

A cross-section image of the G/M/G membrane is shown in Figure 1D, and the G/M/G heterostructure formed by,multiple filtration was consistent with the layered structure of the shellfish biological structure shown in Figure 1A. A nano indentation test was performed (Figure 1E) to characterize the mechanical properties in order to understand the improvement of the elastic modulus

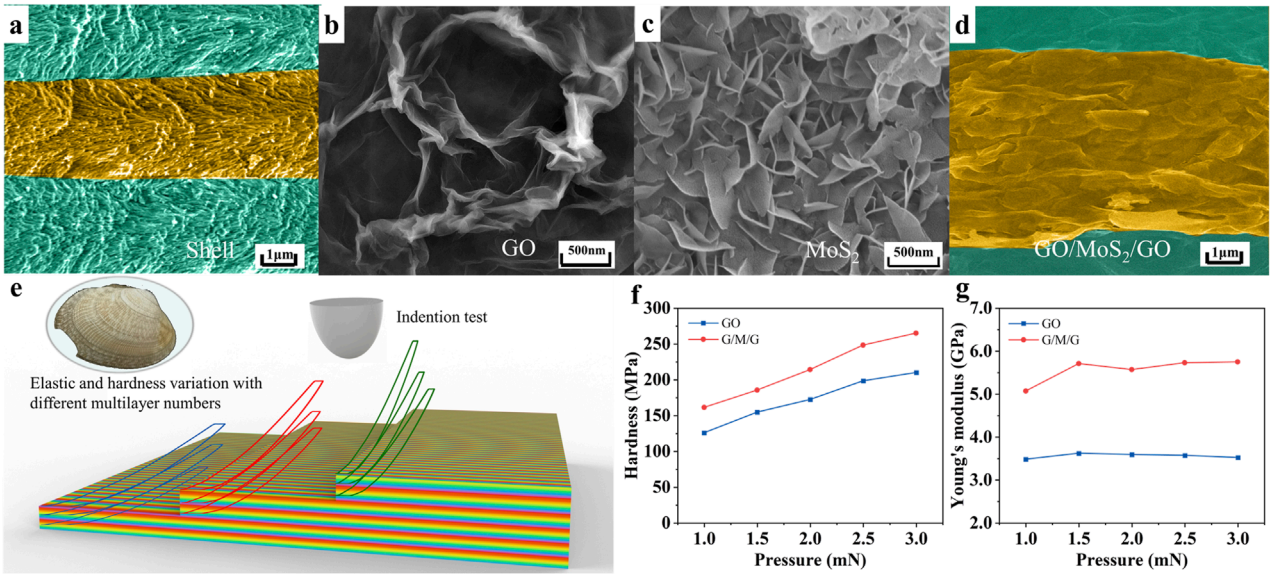

FIGURE 1
SEM images of **(A)** shell structure, **(B)** GO, **(C)** MoS_2, and **(D)** G/M/G membranes. **(E)** Schematic diagram of elastic and hardness variation with different numbers of shell structure layers in indention test. Variations of **(F)** hardness and **(G)** Young's modulus of GO and G/M/G sensors with different pressure.

and toughness of the G/M/G structure with the increased number of layers. The variations in hardness with indent pressure for GO and G/M/G membrane with shell structure (Figure 1F) were respectively 125–211 MPa and 146–272 MPa, indicating 15%–29% enhancement. Variations in Young's modulus with indent pressure for GO membrane and G/M/G membrane with shell structure were 3.48–3.62 GPa and 5.10–5.72 GPa (Figure 1G) indicating an increase by 64%, mostly originating from the G/M/G structure with bionic design. Element analysis of the GO membrane was performed by energy dispersive spectroscopy (EDS; DIGVIVE 5, AMETEK, United States) to obtain the element distribution and atomic proportions.

2.3 Fabrication

Figure 2 diagrams the fabrication procedure of the sensor. The dispersion and diameter of the graphene oxide nanosheet are 2 mg/mL and 0.2–5 μm, respectively, while the dispersion and diameter of the MoS_2 nanosheet are 0.1 mg/mL and 0.2–10 μm, respectively. The filter used in the experiment is an aqueous filter paper with a pore size of 0.22 μm, and the power of the vacuum pumping filtration is 60 L/min. In the fabrication of graphene oxide sensors, 10 mL dispersion liquid was added to 40 mL water for ultrasonic dispersion, after that filtration was performed at the amount of 10 mL per time. The MoS_2 dilution contains two steps: 20 mL dispersion was added to 20 mL water for ultrasonic dispersion, and then 15 mL was taken for filtration each time. After the first filtration of graphene oxide, MoS_2 was flowed very slowly into the filtration device, during which the filter was kept working continuously, so that a layered filtration could be accomplished. The diluted graphene oxide dispersion and MoS_2 dispersion were sequentially filtered using a vacuum filtration device to obtain the filter where the G/M/G structures was attached. Afterwards, the filter was immersed in an organic solvent (ethanol) where the G/M/G film was separated from the filter. Finally, the exfoliated film was transferred to a PDMS substrate with silver electrodes for encapsulation to obtain the sensor device for testing. As shown in the figure, the fabricated sensor has a sandwich structure with the top plate, dielectric medium and bottom plate being the PDMS/Ag, G/M/G and PDMS/Ag, respectively.

2.4 Sensing measurements

The sensing measurement platform (Figure 3A) consisted of a PC, LCR digital bridge (VC4090A, Shengli Company, China), push–pull gauge (digital display, Handpi Company, China), and comprehensive experimental worktop and sensor, and the membrane on the filter membrane transferred to PDMS was connected to platinum wires with good conductivity from spin-coating the conductive silver paste. A working diagram of the test bed under zero strain after the circuit is connected is shown in Figure 3B. A vertically downward external load was applied with accuracy of 0.01 N, and changes in capacitance with increasing pressure of GO/PDMS and G/M/G/PDMS sensors were easily obtained from the LCR digital bridge with measurement accuracy of 0.01 pf (Figure 3C). By placing the sensor on the worktop, the flexible pressure sensing testing device was used to achieve different levels of tensile strain through the cross-feed of the fixture worktop, then the sensitivity of the GO and G/M/G sensors was measured by the LCR digital bridge. The G/M/G/PDMS sensor was used to detect the placement and removal of ultra-small weights such as leaves of different sizes and biological signals such as thumb raising, "yeah", and fist clenching.

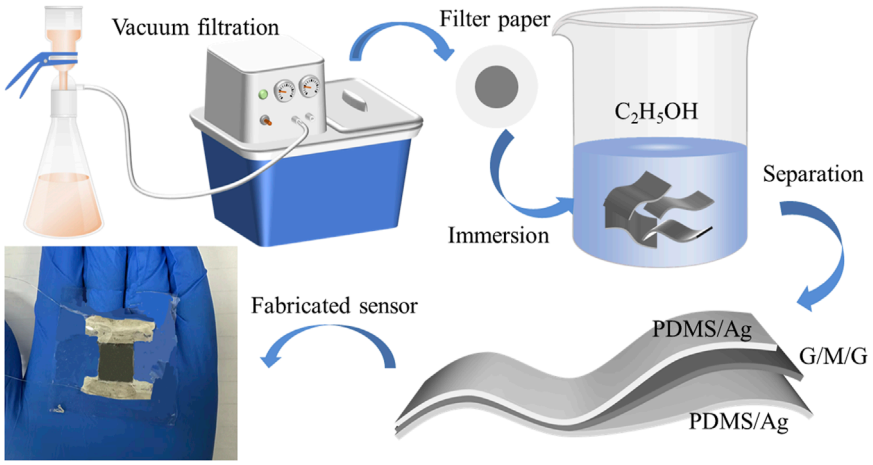

FIGURE 2
Sensor fabrication process.

2.5 DFT modeling

As is well known, MoS_2 and GO membranes are considered as 2H phase and hexagonal structures for commercial materials. The ratio of C and O atoms in the GO membrane could be easily determined as 2:1 according to the EDS characterization (Figure 3D). Therefore, the supercells of GO and GO/MoS_2/GO constructed for DFT calculations were consistent with the materials and structures in our experiments. DFT simulations of band structures of GO and GO/MoS_2/GO were performed by the Vienna Ab initio Simulation Package (VASP) with frozen-core projector-augmented-wave (PAW) pseudopotentials (Kresse and Furthmuller, 1996; Kresse and Joubert, 1999). The exchange correlation potentials were treated by Perdew–Burke–Ernzerhof (PBE) parameterization within the general gradient approximation (GGA) (Perdew et al., 1996). A vacuum region of 15 Å was introduced to avoid interactions between periodic images of slabs. A kinetic energy cutoff of 400 eV was adopted for the plane-wave expansion, and the energy convergence criterion for the self-consistent cycle was 1×10^{-5} eV. All structures were fully relaxed until the force on each atom was below 0.01 eV $Å^{-1}$. In the structural optimization and self-consistent calculations, the k-point sampling mesh was set at $4 \times 4 \times 4$ and $1 \times 4 \times 1$ for band structures of GO and GO/MoS_2/GO, respectively.

3 Results and discussion

After a vertical downward external load of the push–pull force meter was applied to the GO/PDMS and G/M/G/PDMS sensors, the capacitance pressure response curves were easily recorded by the LCR digital bridge (Figure 3C). The blue square and red circle denote relative capacitance change $\triangle C/C_0$ under different external loads, and the slope of the curves, calculated by $(\Delta C/C_0)/P$ and labeled with dashed lines, represents the sensitivity of the GO/PDMS sensor at 0.74 and 0.13 kPa^{-1} and G/M/G/PDMS sensor at 1.60 and 0.28 kPa^{-1}, respectively. The sensitivity of the G/M/G/PDMS sensor at the entire pressure range is obviously higher than that of the GO/PDMS sensor, indicating enhanced sensitivity as a result of the shellfish heterostructure. The change in relative capacitance increases with increasing pressure, and sensitivity is higher in the low pressure range of 0–2 kPa than the high pressure range of 2–7 kPa, which is in agreement with the reported results. To understand the mechanism of enhanced sensitivity caused by shellfish heterostructure, supercells of GO and GO/MoS_2/GO were constructed for DFT modeling, and the initial energy band structures under zero strain were calculated, as shown in Figures 3E, F.

The energy band gap of the former (2.05 eV) is obviously larger than that of the latter (1.66 eV). Because the low band gap leads to high conductivity and small capacitance (Du et al., 2019), the sensitivity of the G/M/G structure was enhanced compared with the GO sensor. This result is in good agreement with a previous report (Lin et al., 2019).

The test device for two-point bending flexible pressure sensing is shown in Figure 4A, and the strain loading device is based on the formula $\varepsilon = (d\sin\theta/2a) \times 100\%$, where d, θ and a refer to the thickness, angle of bending and end-to-end length of the sensor, respectively (Chen et al., 2021). Tensile strains in the range of 1.4%–3.5% are achieved by adjusting the intersection angles of the PDMS plate and horizontal plane in the range of 25°–65°.

The pressure capacitance response curves of GO/PDMS and G/M/G/PDMS sensors are given in Figures 4B, C, which show reduced sensitivity from 0.2 to 0.14 kPa^{-1} and 0.63 to 0.31 kPa^{-1}, respectively. It is clear that the sensitivity of not only GO sensors but also GMG sensors decreases with increasing tensile strain less than 3.5%, which can be well explained by the parallel plate capacitance model (Gong et al., 2017). Notably, the G/M/G heterostructured sensors resisted strains better than the conventional monolayered structures, with a significant increase in sensitivity of 44%–112% over the same strain range.

As shown in Figure 5A, strain greater than 5% was achieved through the cross-feed of the fixture table, in which the middle part of GO and G/M/G sensors on PDMS plates was narrowed. The strain received by the sensor at this point can be calculated

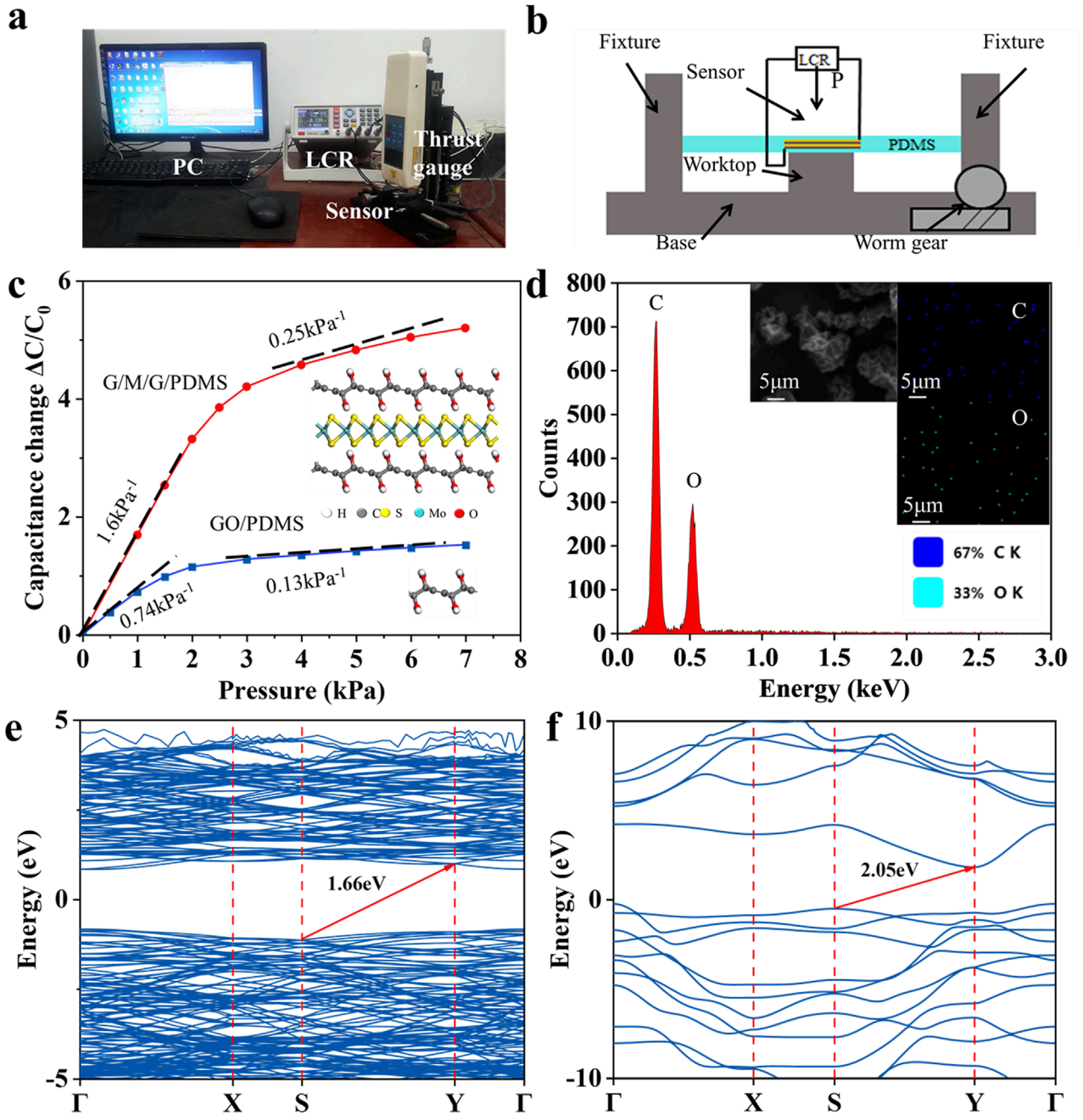

FIGURE 3
(A) Schematic diagram of sensing measurement. **(B)** Working diagram of flexible pressure sensing testing device under zero strain. **(C)** Capacitance change vs. pressure curves of GO and G/M/G heterojunctions. Inset: supercells of GO and GO/MoS_2/GO for DFT calculations. **(D)** EDS element analysis of GO membrane. Initial energy band structures of **(E)** GO and **(F)** G/M/G.

according to the traditional parallel plate stretching formula, i.e., $\varepsilon = (\Delta L/L) \times 100\%$. The pressure capacitance response curves under larger tensile strain in the range of 5%–50% are given in Figures 5B,C for the GO/PDMS and G/M/G/PDMS sensors. By comparison, the sensitivity of GO/PDMS and G/M/G/PDMS sensors was 0.34 and 1.06 kPa^{-1} at 5% strain, and they dropped to 0.19 kPa^{-1} at 40% strain and 0.28 kPa^{-1} at 50% strain. The sensitivity of G/M/G/PDMS sensors at different tensile strain levels is relatively well known in the field of flexible sensors based on PDMS (Wan et al., 2017). It can be concluded that the sensitivity of the G/M/G/PDMS sensor was 75%–102% higher than that of the GO sensor at strain greater than 5%, and the work scope of strain sensing of the G/M/G/PDMS sensor increased to 50%, far more than the 40% for the single-layer GO/PDMS sensor.

To understand the mechanism of enhanced sensitivity and enlarged strain sensing scope, surface profile variation, crack initiation, and propagation were recorded by SEM while continuously increasing strain was applied to the horizontal

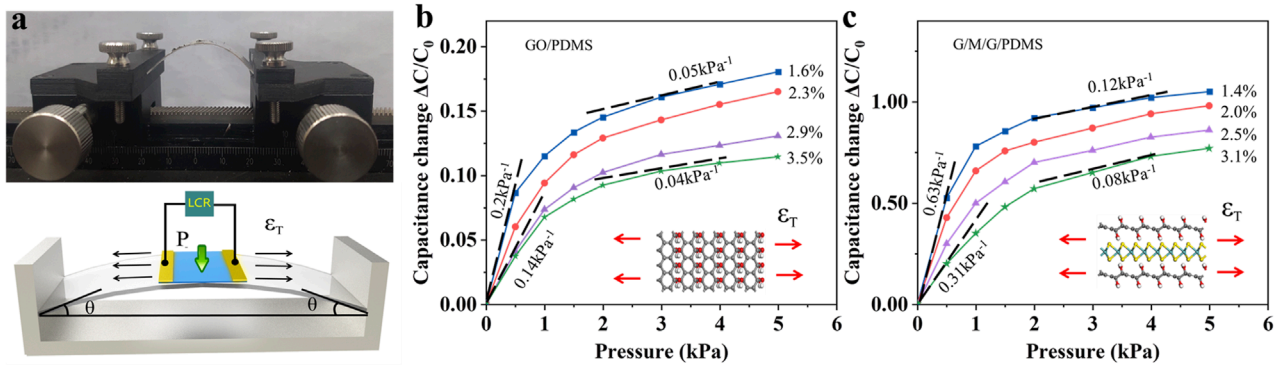

FIGURE 4
(A) Diagram of two-point bending test. Sensitivity of **(B)** GO/PDMS and **(C)** G/M/G/PDMS sensors under tensile strain less than 5%.

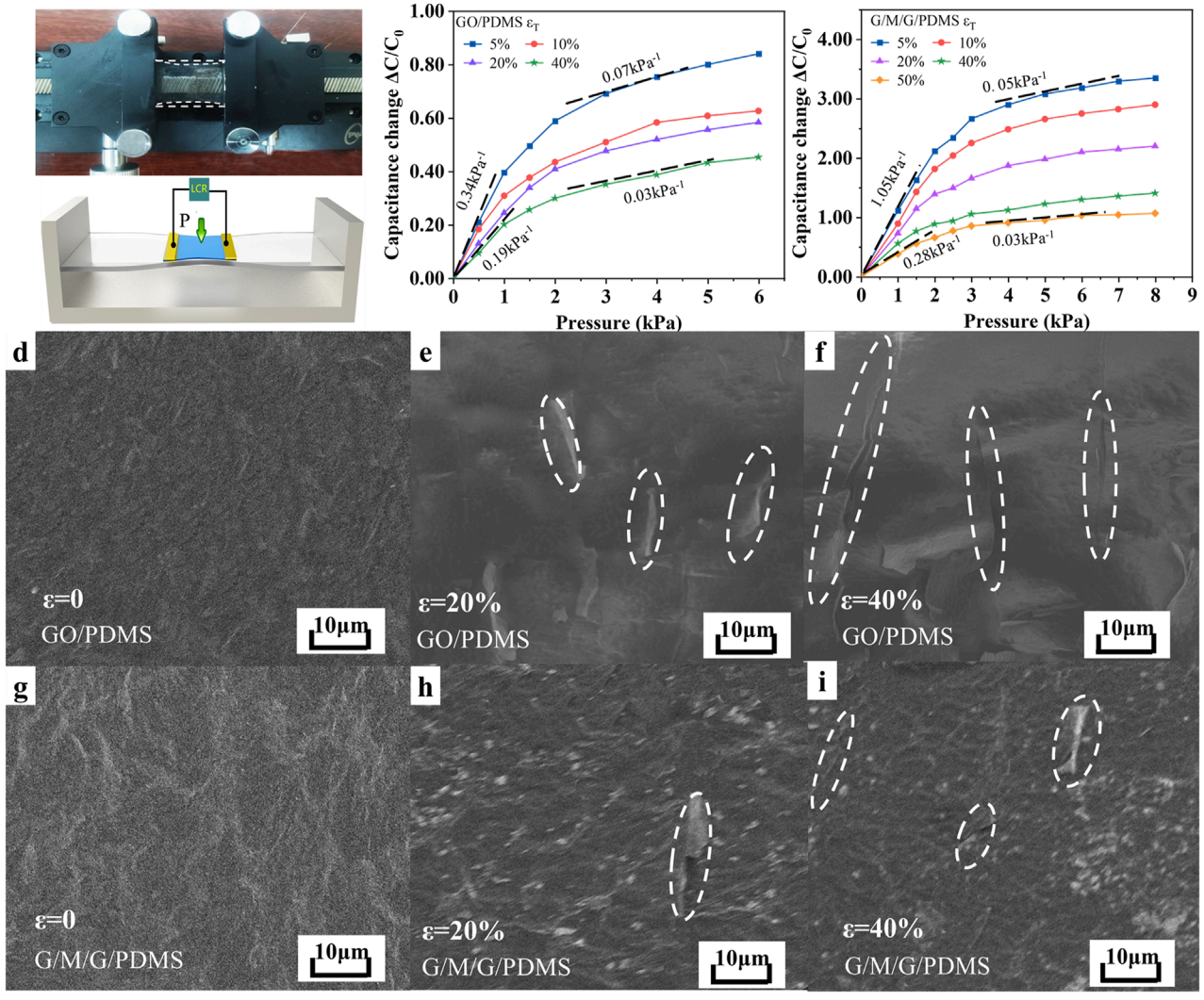

FIGURE 5
(A) Diagram of tensile test. Sensitivity of **(B)** GO/PDMS and **(C)** G/M/G/PDMS sensors under large tensile strain in the range of 5%–50%. Surface images of **(D–F)** GO/PDMS and **(G–I)** G/M/G/PDMS sensors at 0%, 20%, and 40% tensile strain.

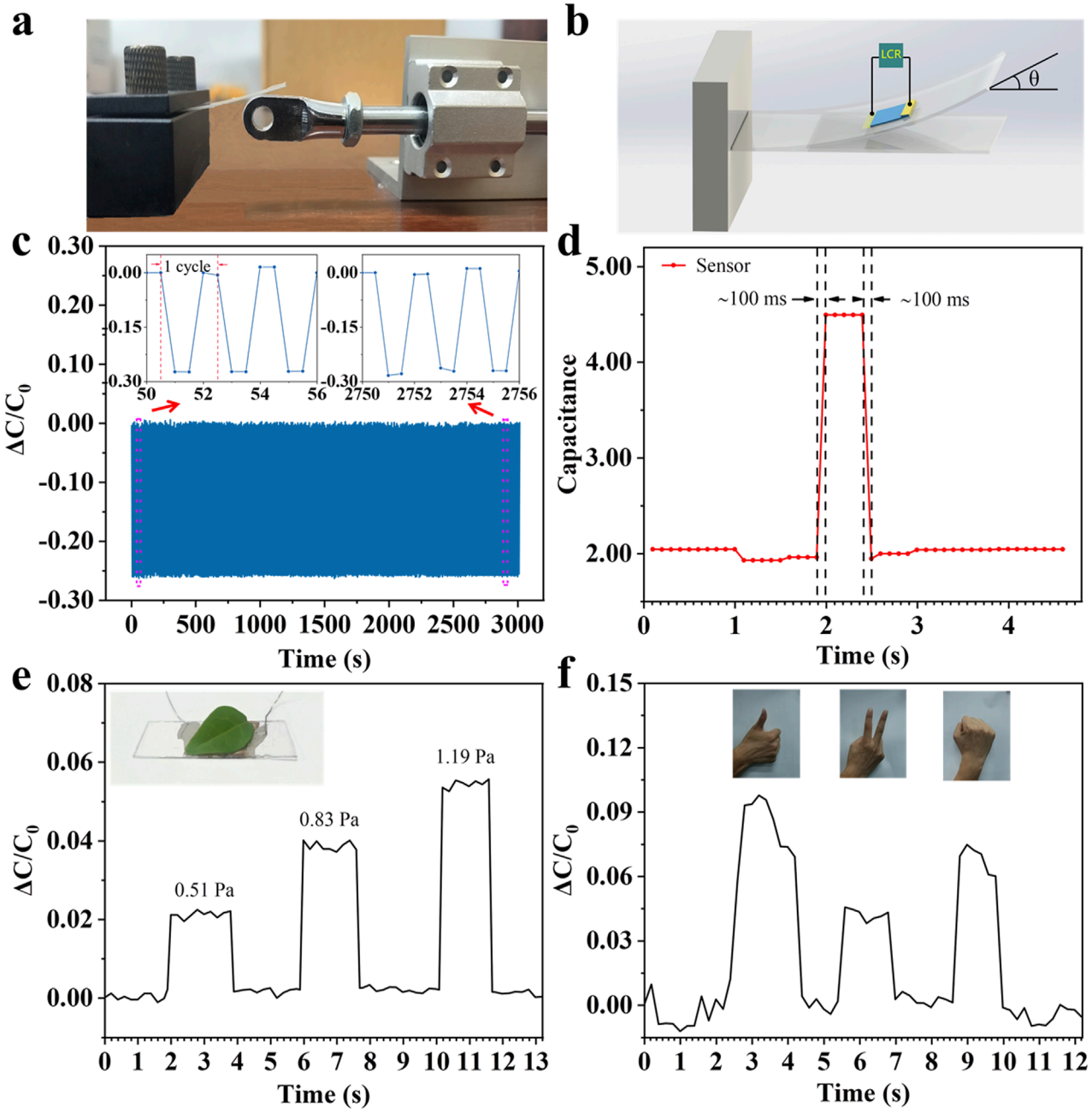

FIGURE 6
(A) Diagram of flexing durability test. **(B)** Working diagram of flexible pressure sensing test by bending sensor at an angle between horizontal and bending direction for loading–unloading cycles. **(C)** Capacitance of G/M/G/PDMS sensor with 1,500 cycles of loading–unloading. Properties of G/M/G/PDMS sensor with shellfish heterostructure, including **(D)** response time, **(E)** transient response to placement and removal of ultra-small weights (leaves, as shown in inset) on the sensor, and **(F)** performance of gesture monitoring.

planes of two sensors, and the typical surface images at 0%, 20%, and 40% tensile strain along the horizontal direction are given in Figures 5D–F for the GO/PDMS sensor and Figures 5G–I for the G/M/G/PDMS sensor. Without strain applied, the two surfaces of the GO/PDMS and G/M/G/PDMS sensors are very dense without any holes (Figures 5D, G). With 20% tensile strain, continuous fractures emerged in the planar regions, while cracks propagated in the textured regions (Figures 5E, H). The number of cracks in the G/M/G/PDMS sensor was obviously smaller than in GO/PDMS sensor. At the same time, the crack initiation and propagation of both sensors was about 90° relative to the horizontal direction, indicating that the cracks were caused by tensile stress. When the tensile strain was increased to 40%, the surface cracks of the GO/PDMS sensor (Figure 5F) became slightly longer compared to the G/M/G/PDMS sensor (Figure 4I), and the continuous propagation along the 90° direction indicates a

uniform tensile fracture along across the section. Slower crack propagation can sustain higher uniaxial strain, because the crack propagation brings about the conductive path of the nano-layer to be cut off (Yang et al., 2022). Therefore, the work scope of strain sensing increased to 50% for the G/M/G/PDMS sensor, which is far more than the 40% for the single-layer GO/PDMS sensor, as shown in Figures 5B, C.

The flexing durability of the G/M/G/PDMS sensor was also tested by bending the sensor to an angle of ~30° between the horizontal and bending directions (Figure 6A) for a thousand cycles, with one end kept fixed with bending in relation to the angle of the other end (Figure 5B). The capacitance change of 1,500 cycles for loading–unloading is given in Figure 5C, and the insets provide enlarged views of the capacitance variations in the ranges of 50–56 s and 2,750–2,756 s. Obvious minimal fluctuations are observed in both the compression and bending results, and the performance loss of the device is less than 1% after 1,500 loading–unloading cycles. This result indicates that there was no fatigue and deterioration of the G/M/G/PDMS sensor with a biological shell structure during 1,500 cycles, which confirms the durability of the biomimetic sensor based on PDMS.

The pressure-sensing properties of the G/M/G/PDMS sensor with shellfish heterostructure were measured by using the LCR meter at an operating frequency 1 kHz (Figures 3A, B), including response time, transient response to the placement and removal of ultra-small weights, and performance of gesture monitoring (Figures 6D–F). There was an instant response to external loading and unloading (Figure 6D), and the response and relaxation time of the G/M/G/PDMS sensor was approximately 100 m, reaching the resolution limit of most testing instruments. As shown in Figure 6E, the sensor could detect the placement and removal of several ultra-small weights. For instance, leaves with different weights (2.5, 4.15, and 6 mg, corresponding to pressure of 0.51, 0.83, and 1.19 Pa, respectively) were placed on and removed from a thin square glass plate covering the entire sensing area. The pressure detection limit of our sensors is 0.51 Pa, which is close to the lowest pressure of 0.24 Pa detected by capacitive pressure sensors as far as we know (Wan et al., 2017). The sensor was placed on the wrist and anchored with tape to monitor gesture performance such as thumb raising, "yeah", and fist clenching using a pressure sensor, as shown in Figure 6F. After processing the signals, it was found that the sensor attached to the wrist successfully detected various body movements, therefore the G/M/G/PDMS sensor can be used effectively for sensing gesture motion.

4 Conclusion

G/M/G filtered thin films with shell-like heterostructure were successfully prepared, and a two-point strain sensing test device based on strain engineering was designed to measure the capacitance–pressure response sensitivity of pressure capacitance sensors under different strain levels. Due to the excellent stiffness and Young's modulus of the bionic shell structure, the sensitivity of G/M/G/PDMS sensors under different levels of strain was much higher compared to the conventional GO sensors, and realized accurate measurement of pressure-sensitive properties with an extended strain measurement range. The changes in sensitivity of G/M/G/PDMS and GO/PDMS flexible pressure sensors at zero strain and tensile strain less than and greater than 5% can be reasonably explained by band theory in DFT simulation, parallel plate capacitor model, and crack growth theory. No fatigue or deterioration were detected in the biological shell structure of the G/M/G/PDMS sensor, and the performance loss of gesture monitoring was less than 1% after 1,500 loading–unloading cycles. The pressure sensor based on G/M/G/PDMS proposed in this article has excellent sensitivity, reliable service life, and a large strain working range; It has broad application potential in fields such as ultra-low pressure monitoring, biological research, and wearable human health monitoring. For example, wrist pulse monitoring and finger joint motion monitoring in smart wearable devices; Alternatively, sensors can be used to monitor finger tapping for early identification of Parkinson's disease.

Data availability statement

The original contributions presented in the study are included in the article/supplementary material, further inquiries can be directed to the corresponding author.

Author contributions

ZH: Conceptualization, Data curation, Formal Analysis, Funding acquisition, Investigation, Methodology, Project administration, Resources, Software, Supervision, Validation, Visualization, Writing–original draft. DZ: Methodology, Resources, Software, Writing–review and editing. YZ: Data curation, Writing–original draft.

Funding

The author(s) declare that financial support was received for the research, authorship, and/or publication of this article. This work was partly supported by Natural Science Foundation of Hunan Province (Grant No.2022JJ30569).

Conflict of interest

The authors declare that the research was conducted in the absence of any commercial or financial relationships that could be construed as a potential conflict of interest.

Publisher's note

References

Artero, V. (2017). Bioinspired catalytic materials for energy-relevant conversions. *Nat. Energy.* 2, 17131. doi:10.1038/nenergy.2017.131

Bhushan, B. (2009). Biomimetics: lessons from nature-an overview. *Phil. Trans. R. Soc. A* 367, 1445–1486. doi:10.1098/rsta.2009.0011

Cao, M. H., Su, J., Fan, S. Q., Qiu, H. W., Su, D. L., and Li, L. (2021). Wearable piezoresistive pressure sensors based on 3D graphene. *Chem. Eng. J.* 406, 126777. doi:10.1016/j.cej.2020.126777

Chen, W., Liu, L. X., Zhang, H. B., and Yu, Z. Z. (2021). Kirigami-inspired highly stretchable, conductive, and hierarchical $Ti_3C_2T_x$ MXene films for efficient electromagnetic interference shielding and pressure sensing. *ACS Nano* 15, 7668–7681. doi:10.1021/acsnano.1c01277

Chen, X. M., Cheng, S. Y., Wen, K. Q., Wang, C. J., Zhang, J., Zhang, H., et al. (2023a). *In-situ* damage self-monitoring of fiber-reinforced composite by integrating self-powered ZnO nanowires decorated carbon fabric. *Compos. Part B* 248, 110368. doi:10.1016/j.compositesb.2022.110368

Chen, X. M., Hui, Y. Z., Zhang, J. B., Wang, Y. L., Zhang, J., Wang, X., et al. (2023b). Single multifunctional MXene-coated glass fiber for interfacial strengthening, damage self-monitoring, and self-recovery in fiber-reinforced composites. *Compos. Part B* 259, 110713. doi:10.1016/j.compositesb.2023.110713

Chun, S., Jung, H., Choi, Y., Bae, G., Kil, J. P., and Park, W. (2015). A tactile sensor using a graphene film formed by the reduced graphene oxide flakes and its detection of surface morphology. *Carbon* 94, 982–987. doi:10.1016/j.carbon.2015.07.088

Du, L. N., Wang, C., Xiong, W. Q., Wei, B., Yang, F. Y., Chen, S. Y., et al. (2019). Strain-induced band-gap tuning of 2D-SnSSe flakes for application in flexible sensors. *Adv. Mat. Technol.* 5, 1900853. doi:10.1002/admt.201900853

Gao, Y., Xiao, T., Li, Q., Chen, Y., Qiu, X. L., Liu, J. W., et al. (2022). Flexible microstructured pressure sensors: design, fabrication and applications. *Nanotechnology* 33, 322002. doi:10.1088/1361-6528/ac6812

Gong, X. X., Fei, G. T., Fu, W. B., Fang, M., Gao, X. D., Zhong, B. N., et al. (2017). Flexible strain sensor with high performance based on PANI/PDMS films. *Org. Elec.* 46, 51–56. doi:10.1016/j.orgel.2017.05.001

Ha, M., Lim, S., Park, J., Um, D. S., Lee, Y., and Ko, H. (2015). Bioinspired interlocked and hierarchical design of ZnO nanowire arrays for static and dynamic pressure-sensitive electronic skins. *Adv. Funct. Mat.* 25, 2841–2849. doi:10.1002/adfm.201500453

Huang, X., Liu, Y. H., Cheng, H. Y., Shin, W. J., Fan, J. A., Liu, Z. J., et al. (2014). Materials and designs for wireless epidermal sensors of hydration and strain. *Adv. Funct. Mat.* 24, 3846–3854. doi:10.1002/adfm.201303886

Isapour, G., and Lattuada, M. (2018). Bioinspired stimuli-responsive color-changing systems. *Adv. Mat.* 30, 1707069. doi:10.1002/adma.201707069

Jiang, J. W., and Park, H. S. (2014). Mechanical properties of MoS_2/graphene heterostructures. *Appl. Phys. Lett.* 105, 033108. doi:10.1063/1.4891342

Kresse, G., and Furthmuller, J. (1996). Efficient iterative schemes for *ab initio* total-energy calculations using a plane-wave basis set. *Phys. Rev. B* 56, 11169–11186. doi:10.1103/physrevb.54.11169

Kresse, G., and Hafner, J. (1993). *Ab initio* molecular dynamics for open-shell transition metals. *Phys. Rev. B* 48, 13115–13118. doi:10.1103/physrevb.48.13115

Kresse, G., and Joubert, D. (1999). From ultrasoft pseudopotentials to the projector augmented-wave method. *Phys. Rev. B* 59, 1758–1775. doi:10.1103/physrevb.59.1758

Lee, J., Kwon, H., Seo, J., Shin, S., Koo, J. H., Pang, C., et al. (2015). Conductive fiber-based ultrasensitive textile pressure sensor for wearable electronics. *Adv. Mat.* 27, 2433–2439. doi:10.1002/adma.201500009

Li, R. Q., Zhou, Q., Bi, Y., Cao, S. J., Xia, X., Yang, A. L., et al. (2020). Research progress of flexible capacitive pressure sensor for sensitivity enhancement approaches. *A-Phys.* 321, 112425. doi:10.1016/j.sna.2020.112425

Lin, P., Zhu, L., Li, D., Xu, L., Pan, C., and Lin, Z. (2019). Piezo-Phototronic Effect for Enhanced Flexible MoS_2/WSe_2 van der Waals Photodiodes. *Adv. Funct. Mat.* 28, 1802849. doi:10.1002/adfm.201802849

Mannsfeld, S. C. B., Tee, B. C. K., Stoltenberg, R. M., Chen, C. V. H. H., Barman, S., Muir, B. V. O., et al. (2013). Highly sensitive flexible pressure sensors with microstructured rubber dielectric layers. *Nat. Mat.* 9, 859–864. doi:10.1038/nmat2834

Mao, L. B., Gao, H. L., Yao, H. B., Liu, L., Colfen, H., Liu, G., et al. (2016). Synthetic nacre by predesigned matrix-directed mineralization. *Science* 354, 107–110. doi:10.1126/science.aaf8991

Michelis, F., Bodelot, L., Bonnassieux, Y., and Lebental, B. (2015). Highly reproducible, hysteresis-free, flexible strain sensors by inkjet printing of carbon nanotubes. *Carbon* 95, 1020–1026. doi:10.1016/j.carbon.2015.08.103

Nesser, H., and Lubineau, G. (2021). Strain sensing by electrical capacitive variation: from stretchable materials to electronic interfaces. *Adv. Electron. Mat.* 7, 2100190. doi:10.1002/aelm.202100190

Pan, L. J., Chortos, A., Yu, G. H., Wang, Y. Q., Isaacson, S., Allen, R., et al. (2014). An ultra-sensitive resistive pressure sensor based on hollow-sphere microstructure induced elasticity in conducting polymer film. *Nat. Commun.* 5, 3002. doi:10.1038/ncomms4002

Pang, C., Lee, G. T., Kim, T. I., Kim, S. N., Kim, H. N., Ahn, S. H., et al. (2012). A flexible and highly sensitive strain-gauge sensor using reversible interlocking of nanofibres. *Nat. Mat.* 11, 795–801. doi:10.1038/nmat3380

Parida, K., Bhavanasi, V., Kumar, V., Bendi, R., and Lee, P. S. (2017). Self-powered pressure sensor for ultra-wide range pressure detection. *Nano Res.* 10, 3557–3570. doi:10.1007/s12274-017-1567-6

Park, S. J., Kim, D. W., Jang, S. W., Jin, M. L., Kim, S. J., Ok, J. M., et al. (2016). Fabrication of graphite grids via stencil lithography for highly sensitive motion sensors. *Carbon* 96, 491–496. doi:10.1016/j.carbon.2015.09.080

Perdew, J. P., Burke, K., and Ernzerhof, M. (1996). Generalized gradient approximation made simple. *Phys. Rev. B* 77, 3865–3868. doi:10.1103/physrevlett.77.3865

Qin, J., Yin, L. J., Hao, Y. N., Zhong, S. L., Zhang, D. L., Bi, K., et al. (2021). Flexible and stretchable capacitive sensors with different microstructures. *Adv. Mat.* 33, 2008267. doi:10.1002/adma.202008267

Schwartz, G., Tee, B. C. K., Mei, J. G., Appleton, A. L., Kim, D. H., Wang, H. L., et al. (2013). Flexible polymer transistors with high pressure sensitivity for application in electronic skin and health monitoring. *Nat. Commun.* 4, 1859. doi:10.1038/ncomms2832

Sun, Z. Q., Liao, T., Li, W., Qiao, Y., and Ostrikov, K. (2019). Beyond seashells: bioinspired 2d photonic and photoelectronic devices. *Adv. Funct. Mat.* 29, 1901460. doi:10.1002/adfm.201901460

Takei, K., Takahashi, T., Ho, J. C., Ko, H., Gillies, A. G., Leu, P. W., et al. (2010). Nanowire active-matrix circuitry for low-voltage macroscale artificial skin. *Nat. Mat.* 9, 821–826. doi:10.1038/nmat2835

Troullier, N., and Martins, J. L. (1991). Efficient pseudopotentials for plane-wave calculations. *Phys. Rev. B* 43, 1993–2006. doi:10.1103/physrevb.43.1993

Wan, S., Bi, H. C., Zhou, Y. L., Xie, X., Su, S., Yin, K. B., et al. (2017). Graphene oxide as high-performance dielectric materials forcapacitive pressure sensors. *Carbon* 14, 209–216. doi:10.1016/j.carbon.2016.12.023

Wegst, U. G. K., Bai, H., Saiz, E., Tomsia, A. P., and Robert, O. (2015). Ritchie bioinspired structural materials. *Nat. Mat.* 14, 23–26. doi:10.1038/NMAT4089

Wu, L., Li, X., Choi, J., Zhao, Z. J., Qian, L. M., Yu, B. J., et al. (2024). Beetle-inspired gradient slant structures for capacitive pressure sensor with a broad linear response range. *Adv. Funct. Mat.* 34, 2312370. doi:10.1002/adfm.202312370

Xu, F. L., Li, X. Y., Shi, Y., Li, L. H., Wang, W., He, L., et al. (2018). Recent developments for flexible pressure sensors:a review. *Micromachines* 9, 580. doi:10.3390/mi9110580

Yang, H. T., Li, J. L., Xiao, X., Wang, J. H., Li, Y. F., Li, K. R., et al. (2022). Topographic design in wearable MXene sensors with in-sensor machine learning for full-body avatar reconstruction. *Nat. Commun.* 13, 5311. doi:10.1038/s41467-022-33021-5

Yang, J., Luo, S., Zhou, X., Li, J. L., Fu, J. T., Yang, W. D., et al. (2019). Flexible, tunable, and ultrasensitive capacitive pressure sensor with microconformal graphene electrodes. *ACS Appl. Mat.* 11, 14997–15006. doi:10.1021/acsami.9b02049

Zhang, C. Q., Mcadams, D. A., and Grunlan, J. C. (2016). Nano/micro-manufacturing of bioinspired materials: a review of methods to mimic natural structures. *Adv. Mat.* 28, 8566–6321. doi:10.1002/adma.201604494

Zhang, J., Ye, S. B., Liu, H. L., Chen, X., Chen, X., Li, B., et al. (2020). 3D printed piezoelectric BNNTs nanocomposites with tunable interface and microarchitectures for self-powered conformal sensors. *Nano Energy* 77, 105300. doi:10.1016/j.nanoen.2020.105300

Zhu, Y. S., Li, J. W., Cai, H. B., Wu, Y. M., Ding, H. Y., Pan, N., et al. (2017). Highly sensitive and skin-like pressure sensor based on asymmetric double-layered structures of reduced graphite oxide. *B-Chem.* 255, 1262–1267. doi:10.1016/j.snb.2017.08.116